This is the accepted manuscript made available via CHORUS. The article has been published as:

Impact of the charge density wave state in the electrodynamic response of ZrTe_{3−x}Se_{x}: Optical evidence for a pseudogap phase

M. Chinotti, J. Ethiraj, C. Mirri, Xiangde Zhu, Lijun Li, C. Petrovic, and L. Degiorgi

Phys. Rev. B **97**, 045117 — Published 12 January 2018

DOI: 10.1103/PhysRevB.97.045117

Impact of the charge-density-wave state in the electrodynamic response of $ZrTe_{3-x}Se_x$: optical evidence for a pseudogap phase

M. Chinotti[1], J. Ethiraj[1,+], C. Mirri[1], Xiangde Zhu[2,3], Lijun Li[2,4], C. Petrovic[2], and L. Degiorgi[1]
[1] *Laboratorium für Festkörperphysik, ETH Zürich, CH-8093 Zürich, Switzerland*
[2] *Condensed Matter Physics and Materials Science Department, Brookhaven National Laboratory, Upton, NY 11973, U.S.A.*
[3] *AnHui Province Key Laboratory of Condensed Matter Physics at Extreme Conditions, High Magnetic Field Laboratory, Chinese Academy of Sciences and University of Science and Technology, Hefei 230031, China and*
[4] *Key Laboratory of Materials Physics, Institute of Solid State Physics, Chinese Academy of Sciences, Hefei 230031, China*

(Dated: December 10, 2017)

The emergence of superconductivity upon progressively suppressing the long-range, charge-density-wave (CDW) order characterises the phase diagram of several materials of interest in the on-going solid-state physics research. Se-doped $ZrTe_3$ compounds provide the most recent, suitable arena in order to investigate the interplay of otherwise competing orders in layered-like two-dimensional systems. We present an optical study of the CDW state in $ZrTe_{3-x}Se_x$ at selected Se-doping, based on the measurement of the reflectivity from the far-infrared up to the ultraviolet, as a function of temperature. We particularly focus our attention to the redistribution of the spectral weight, which images the impact of the CDW state within the optical conductivity across the phase diagram of the title compounds. The electrodynamic response is consistent with a scenario based on a long-range CDW condensate at low Se-doping. Upon increasing the Se content, this then gives way to local, short range order CDW segments. Our spectral weight analysis reveals the presence of a pseudogap phase, as fingerprint of the CDW precursor effects and thus shaping the charge dynamics of the title compounds in their normal state, preceding the onset of superconductivity.

PACS numbers: 78.20.-e, 71.30.+h, 71.45.Lr

I. INTRODUCTION

Since the prediction of the Peierls instability mid-fifties of the last century in so-called one-dimensional (1D) systems[1] there has been a great deal of efforts to experimentally recognise the formation of the collective charge-density-wave (CDW) condensate[2]. The 1D systems are particularly favourable since the Fermi surface (FS) nesting supplemented by the electron-phonon coupling set the prerequisite for the onset of a singularity in the Lindhard response function, driving the material into the CDW state characterised by a periodic modulation of the electron charge density. It is a common notion that the Peierls transition induces an electron-hole pairing with $\vec{q} = 2k_F$ (k_F being the Fermi wave vector) and leads to the opening of a gap on FS, signalling the lower energy of the resulting collective ground state. Upon increasing the dimensionality of the electron gas, one can still observe the CDW formation, generally affecting only a portion of FS though; indeed, the remaining ungapped fraction accounts for the metallic nature of these materials.

At high dimensionality, additional quantum states, originating from alternative FS instabilities, may be expected as well. The most prominent example is the superconducting state, due to the pairing of electrons with total $\vec{q} = 0$. This latter quantum state is characterised by infinite conductivity, even though it also features a FS gap. Superconductivity and CDW are believed to be mostly competing orders and two-dimensional (2D) materials are favourable systems in order to study their interplay.

Broken-symmetry competing states, as CDW and superconductivity, have been widely established in the high temperature superconducting cuprates[3–7], so that the CDW state itself advanced as an important ingredient with respect to the onset of superconductivity and may even be intimately related to its pairing mechanism. For instance, a rather recent combination of resonant x-ray scattering, scanning-tunneling microscopy and angle-resolved photoemission spectroscopy experiments reveals the existence of a generic charge-ordered state in underdoped cuprate families and uncovers its intimate connection and ubiquity with the pseudogap regime[7]. This is quite astonishing on its own, since the resistance-free movement of charge carriers in a superconductor may interplay with the rather opposite state characterized by spatial ordering of charges, and brings up the more general issue, as to whether such opposite states could macroscopically coexist or give rise to a phase separation in real space. Consequently, a vigorous search of model materials was initiated in order to address these intertwined broken-symmetry collective states upon tunable parameters (like doping or pressure).

The 2D transition metal (M) MX_2 and MX_3 chalcogenides (X stays for S, Se and Te) provide an interesting playground in order to address the CDW state and, with appropriate chemical doping, even its interplay with su-

perconductivity. As paramount example, we first quote the direct observation of the energy gap in 2H-$NbSe_2$ caused by CDW, as envisaged by using angle-resolved photoemission spectroscopy[8]. The gap opens in the regions of the momentum space connected by the CDW vectors, which implies a nesting mechanism of CDW formation. In remarkable analogy with the pseudogap in cuprates, the detected energy gap also exists in the normal state and it forestalls the superconducting gap by excluding the nested portions of FS from participating in superconductivity.

Quite an extensive experimental effort has been also devoted to $ZrTe_3$, which has a monoclinic structure where the main components are rods formed by $ZrTe_3$ prisms stacked along the b-axis, forming the Zr-Zr chains. Two of such identical rods are then connected by inversion symmetry in the monoclinic cell. Since $ZrTe_3$ is acting as the reference material for the compositions addressed in this study, it is worthwhile to mention its relevant physical properties as well as those of its alloys. This will help setting the stage for the present optical investigation on Se-doped $ZrTe_3$. The temperature (T) dependence of the resistivity $\rho(T)$ of $ZrTe_3$ displays an anomaly due to the CDW state at $T_{CDW} = 63$ K, developing along the crystallographic directions perpendicular to the Zr-Zr chains (i.e., b-axis)[9]. Optical signatures of the CDW condensate are also identified in the infrared spectral range, displaying a mean-field like T-dependence of the CDW single particle gap below and fingerprints of CDW fluctuations above T_{CDW}[10]. By further lowering the temperature below 2 K, filamentary superconductivity has been discovered[11]. A pressure dependent study shows furthermore that superconductivity first disappears above 0.5 GPa but emerges again above 5 GPa, giving evidence of pressure-induced re-entrant superconductivity[12]. Between 0 and 5 GPa, T_{CDW} displays a dome-like behavior and peaks around 2 and 3 GPa. This is quite counterintuitive, since pressure is known to affect the CDW state by modifying the shape of FS. The enhancement of the dimensionality by pressure should suppress the nesting conditions, which would favour CDW, but increases the density of states at the Fermi level, which is an ingredient for superconductivity. Apparently, around 2 to 3 GPa there must be an unconventional and yet not fully understood pressure-induced enhanced nesting of FS, as observed in some low dimensional organic conductors[12].

Furthermore, the intercalation by Ag, Cu and Ni of $ZrTe_3$ has been foreseen as an alternative to externally applied pressure in order to induce superconductivity[13–15]. Recent reports on $Cu_{0.05}ZrTe_3$ and $Ni_{0.05}ZrTe_3$ single crystals indeed bring up evidence for bulk superconductivity below 4 K, apparently coexisting with a CDW state nonetheless affecting different portions of FS[13,14]. Stated differently, both collective states do coexist in real space but must compete for the same FS and therefore do separate in reciprocal space. Within the assumption of homogeneous samples, we achieve a similar conclusion also from the discussion of their optical response[16].

It has been recently claimed that superconductivity emerges in the conducting $ZrTe_3$ when the long-range CDW order is gradually suppressed upon Se doping (inset of Fig. 1(b)). On the one hand, the CDW transition is absent for $x \geq 0.03$. On the other hand, the superconducting critical temperature $T_c(x)$ in $ZrTe_{3-x}Se_x$ ($0 \leq x \leq 0.1$) increases up to the 4 K plateau for $0.04 \leq x \leq 0.07$[17]. Further increase in Se content results in diminishing T_c and filamentary superconductivity. The *dc* resistivity ($\rho(T)$) displays a substantial in-plane anisotropy upon Se-doping and $\rho(T)$ of the high-T_c compositions is linear up to highest measured T= 300 K and turns into a T^2-dependence below $\sim$ 60 K[17]. Despite the fact that the anomaly in the overall metallic *dc* resistivity due to the CDW transition is only observable at low doping x along the a-axis, the CDW related modes from Raman spectra (i.e., the amplitude mode[18]) were also observed for $x = 0.04$ and 0.1 crystals. It has been speculated that Se-doping at least up to the optimal concentration ($0.04 \leq x \leq 0.07$) acts like pressure and thus enhances the 1D-3D band coupling, leading to bulk superconductivity. In addition, it also brings disorder, so that CDW islands survive in the (percolative) superconducting state[17].

We report here on the optical response of $ZrTe_{3-x}Se_x$ for the $x = 0.01$ and 0.06 compositions over a broad spectral range and as a function of temperature. While T_c for the superconducting transition is too low (≤ 4 K) in order to appreciate its direct impact on the optical response, the chosen Se-doping compositions act as model materials, spanning the phase diagram between a compound with a nominal CDW state ($x = 0.01$, with $T_{CDW} \simeq 45$ K) and a sample without any long-range charge ordering ($x = 0.06$) (inset of Fig. 1(b)). Even though sequel to our previous work on $ZrTe_3$[10] as well as on Cu- and Ni-doped $ZrTe_3$[16], the main motivation here is to address the optical fingerprints pertinent to the CDW condensate and the crossover to a regime determined by its fluctuation and/or precursor effects, which all precede superconductivity, along the doping axis of a single compound. The spectral weight distribution as a function of temperature, inferred from the optical conductivity, provides evidence for a pseudogap formation in both compositions at high temperatures. Throughout this paper, we refer to the notion of pseudogap for the excitation resulting from the precursor effects of the broken-symmetry state. This latter excitation then evolves into a CDW single particle (partial) gap for the $x = 0.01$ compound upon further lowering the temperature below T_{CDW}, while for the $x = 0.06$ composition its metallic nature is progressively enhanced, so that the Drude resonance dominates the optical response and particularly overcasts the pseudogap formation. This indicates the relevance of incipient CDW fluctuation across the phase diagram, merging into a long-range charge order at low temperatures only for underdoped Se-compositions.

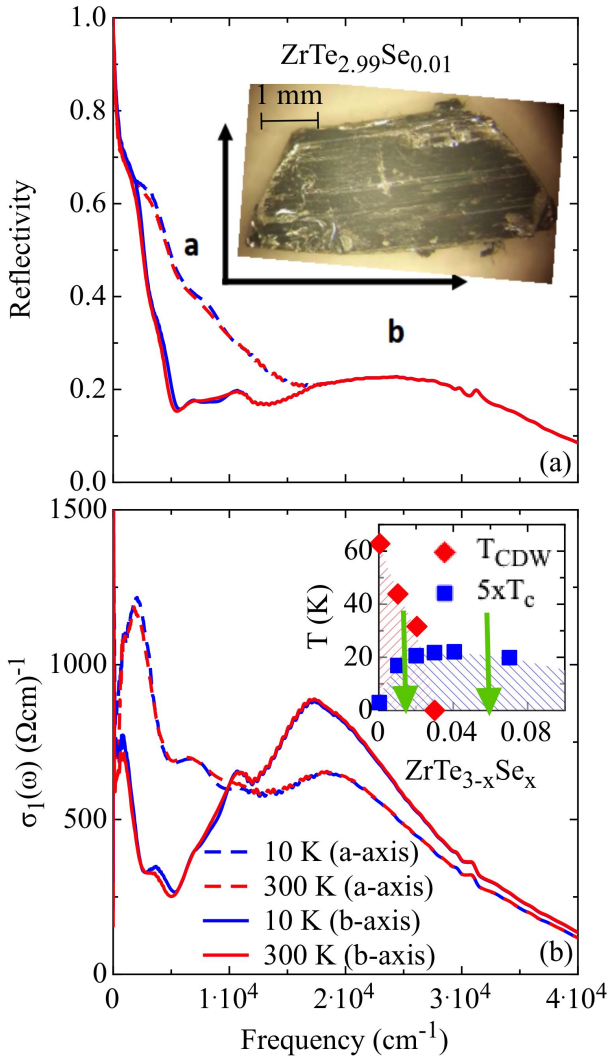

FIG. 1: (color online) (a) Optical reflectivity ($R(\omega)$) and (b) real part ($\sigma_1(\omega)$) of the optical conductivity at 10 and 300 K along the a and b axes of $ZrTe_{2.99}Se_{0.01}$ with $T_{CDW} \simeq 45$ K. The inset in panel (a) shows the specimen with the relevant axes orientation. The inset in panel (b) displays a schematic CDW $T_{CDW}(x)$ and superconducting $T_c(x)$ phase diagram of $ZrTe_{3-x}Se_x$[17], which emphasises the compositions addressed in this study (green arrows).

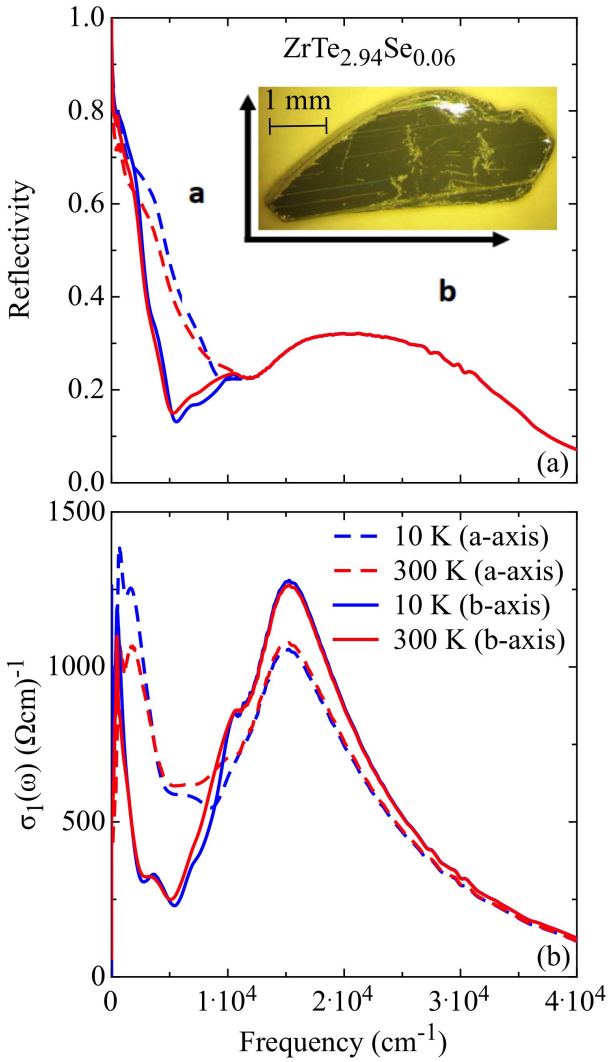

FIG. 2: (color online) (a) Optical reflectivity ($R(\omega)$) and (b) real part ($\sigma_1(\omega)$) of the optical conductivity at 10 and 300 K along the a and b axes of $ZrTe_{2.94}Se_{0.06}$. The inset in panel (a) shows the specimen with the relevant axes orientation.

II. MATERIALS AND EXPERIMENTAL TECHNIQUE

Single crystals of $ZrTe_{3-x}Se_x$ with $x = 0.01$ and 0.06 were grown via iodine vapor transport method[13,14,17]. The as-grown single crystals can be easily cleaved along the b- and c-axis, which usually produces needle- or tape-like crystals along the b-axis in the ab plane (inset of Fig. 1(a) and 2(a)). Elemental analysis was performed by energy-dispersive X-ray spectroscopy (EDS) on an FEI Helios Nanolab 600i in order to determine the Se content. The Se content in as-grown crystals is found to be less than the content in the starting material; measured EDS values are used throughout the paper.

We perform reflectivity ($R(\omega)$) measurements at temperatures between 10 K and 300 K from the far infrared (FIR) up to the mid- and near-infrared spectral range (MIR-NIR) (40-10000 cm^{-1}) by means of a Fourier-transform infrared Bruker Vertex 80v interferometer coupled to an Oxford SM 4000 cryostat. Since the T-dependence of $R(\omega)$ expires by 10^4 cm^{-1}, we can confidently extend the reflectivity data up to the ultraviolet (UV) range ($\omega \sim 40000$ cm^{-1}) by using a PerkinElmer Lambda 950 spectrometer, operating at 300 K. Our fully oriented crystals allow us collecting data with electromagnetic radiation polarized along the in-plane a- and b-axis (inset of Fig. 1(a) and 2(a)). From $R(\omega)$ we extract the real part ($\sigma_1(\omega)$) of the optical conductivity via

Kramers-Kronig (KK) transformation. Since our compositions are metallic at all temperatures, $R(\omega)$ above T_c is extrapolated towards zero frequency via the Hagen-Rubens law (HR) $R(\omega) = 1 - 2\sqrt{\frac{\omega}{\sigma_{dc}}}$, with σ_{dc} values along both axes characterised by a relative temperature dependence in fair agreement with that evinced from *dc* transport measurements[17]. At high frequencies beyond our upper frequency limit, $R(\omega)$ is modelled by the standard expression given by $R(\omega) \sim \omega^{-s}$ with $2 \leq s \leq 4$. Further details pertaining to the measurements can be found in Ref. 18.

III. RESULTS

Figures 1(a) and 2(a) feature the measured optical reflectivity at 10 and 300 K for both polarization directions for the two $x = 0.01$ and 0.06 compositions. First of all, let us compare the optical response of the title compounds with our previous data on $ZrTe_3$[10] and its Cu- and Ni-intercalated compounds[16]. While Ni-intercalation does not dramatically alter the optical response encountered in $ZrTe_3$, it turns out that Cu-intercalation as well as Se-doping affect more strongly the electronic structure of the parent compound. The spectra of Fig. 1 and 2 considerably deviates form that in $ZrTe_3$[10], although similar to the optical properties of $Cu_{0.05}ZrTe_3$.

The first general observation emerging from the spectra in Fig. 1 and 2 is that, despite the two-dimensional structure, the optical response of the title compounds is very much anisotropic between the two crystallographic axes within the *ab*-plane. This images the presence of the quasi-one dimensional trigonal prismatic $ZrTe_6$ chains, which are responsible for the elongated shape of the crystals along the *b*-axis (insets of Fig. 1(a) and 2(a)). The plasma edge feature, at which $R(\omega)$ sharply increases towards total reflection for frequencies towards zero, reveals the metallic nature of both compounds at any temperature. Above the plasma edge (i.e., $\omega > 10^4$ cm^{-1} for the *a*-axis and $\omega > 5000$ cm^{-1} for the *b*-axis) we observe several broad absorption features. Moreover, as it will be elaborated below, we anticipate that several shoulders, overlapped to the plasma edge of $R(\omega)$, lead to rather strong low frequency absorptions, in addition to the metallic contribution of the optical spectra. Therefore, the electronic interband transitions affect the electrodynamic response quite strongly into the infrared range, thus already at energy scales of the order of 70 to 100 meV.

The real part $\sigma_1(\omega)$ of the optical conductivity, shown in Fig. 1(b) and 2(b), first highlights the strong absorptions above 5000 cm^{-1} along both axes and for both materials, which are generally ascribed to electronic interband transitions. Along the *a*-axis there is a strong peak between 1.5x10^4 and 2x10^4 cm^{-1}, while along the *b*-axis there is a similar absorption with an additional shoulder around 10^4 cm^{-1} on its low-frequency tail.

In order to highlight the temperature dependence of the optical conductivity, we show $\sigma_1(\omega)$ at selected temperatures and low frequencies (i.e., $\omega < 5000$ and 12000 cm^{-1} for $x = 0.01$ and 0.06, respectively) in Fig. 3 and 4. We immediately recognise rather strong and temperature dependent absorptions, overlapped to the high-frequency tail of the metallic contribution to $\sigma_1(\omega)$. The latter seems to be less pronounced upon doping with lower $\sigma_1(\omega \to 0)$ at all temperatures, manifesting the induced disorder upon Se-substitution on Te (insets in Fig. 3 and Fig. 4).

Specifically, there is a broad feature peaked at 2000 and 1000 cm^{-1} for $x = 0.01$ along the *a*- and *b*-axis, respectively, before the optical conductivity displays an upturn giving rise to a narrow Drude like resonance in the $\omega \to 0$ limit, which further narrows upon lowering the temperature (insets in Fig. 3). We recognise a T-dependence of $\sigma_1(\omega)$, which implies a reshuffling of spectral weight, as it will be discussed later. This is even more evident for the $x = 0.06$ compound, for which spectral weight get obviously depleted below 10^4 cm^{-1} and piles up in the strong peak centred at approximately 1300 and 500 cm^{-1} along the *a*- and *b*-axis, respectively. Also for this latter compound, $\sigma_1(\omega)$ is finite at *dc* and its $\omega \to 0$ limit gets enhanced upon lowering the temperature (insets in Fig. 4), consistent with the metallic nature of the *dc* transport results. However, the metallic component is rather broad compared to the narrow one for $x = 0.01$, anticipating a larger scattering rate of the itinerant charge carriers in $x = 0.06$ than in x =0.01 (insets in Fig. 3 and Fig. 4). Even though not elaborated in details in the present work, we attempted a phenomenological fit based on a multi-component Drude-Lorentz approach[18]. The best total fit at 10 and 300 K as well as its low frequency components at 300 K are shown in the insets of Fig. 3 and Fig. 4. The width of the Drude resonance is a measure of the scattering rate and is obviously larger for $x = 0.06$ than for $x = 0.01$.

IV. DISCUSSION

The optical anisotropy is common to both compositions, while the details of their T-dependence (Fig. 3 and 4) are different. In order to shed light on the T-dependence of the optical response across the CDW phase diagram studied here (inset of Fig. 1(b))[17], we favor in this work the model-independent analysis of the spectral weight redistribution, instead of the more common data-fit based on the multi-component phenomenological Drude-Lorentz approach[19]. Indeed, the latter would depend on several assumptions concerning the number and position along the energy axis of the various fit components. Moreover, for the analysis of the spectral weight distribution within the phenomenological fit we would be limited to its reshuffling among the fit components in their own spectral range but not to its overall

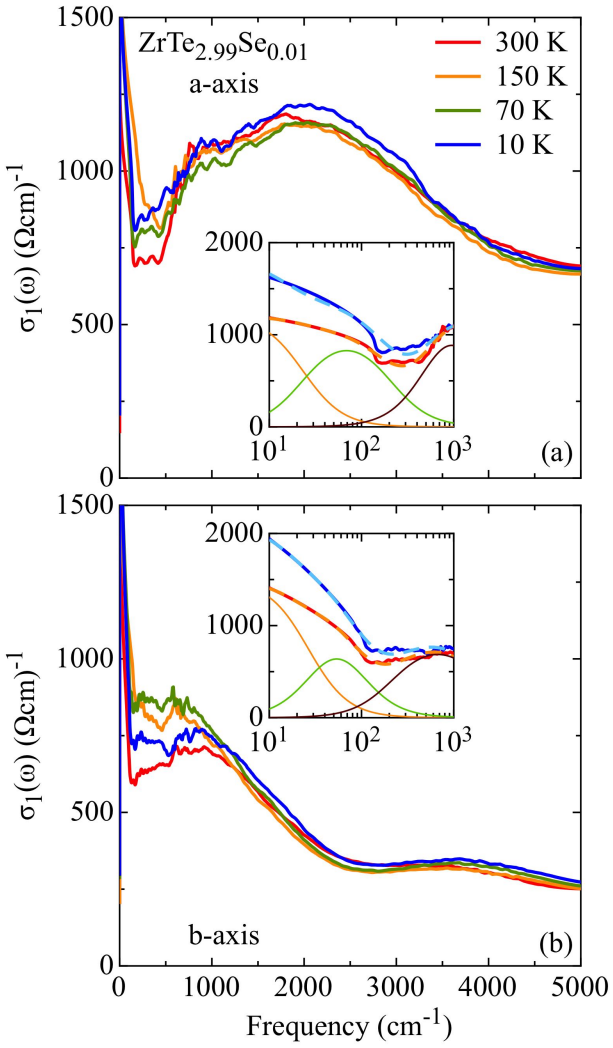

FIG. 3: (color online) Real part ($\sigma_1(\omega)$) of the optical conductivity at selected temperatures along the a (a) and b (b) axes of $ZrTe_{2.99}Se_{0.01}$, emphasising the spectral range below 5000 cm^{-1}. Above 5000 cm^{-1} all spectra for both axes merge together at any temperature. Insets: $\sigma_1(\omega)$ at 10 and 300 K with logarithmic energy scale emphasising the narrowing of the metallic (Drude) component with decreasing T (see text). Thick dashed lines are the total fit after the phenomenological Lorentz-Drude approach[18], while the thin lines display the single fit components at low frequencies (orange: Drude; green and brown: harmonic oscillator). The T-color code is identical in both panels and insets.

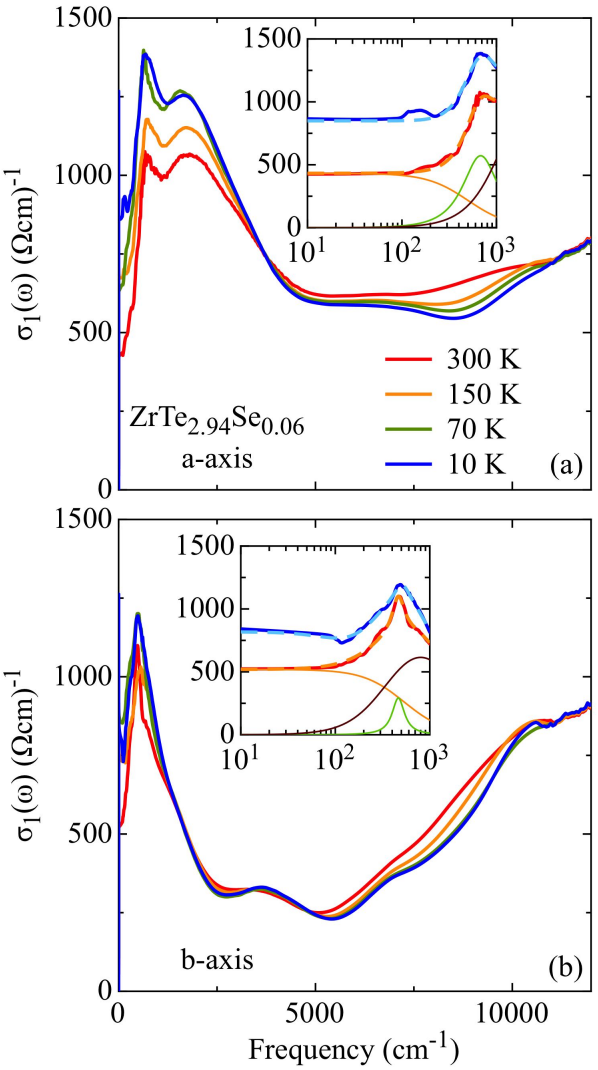

FIG. 4: (color online) Real part ($\sigma_1(\omega)$) of the optical conductivity at selected temperatures along the a (a) and b (b) axes of $ZrTe_{2.94}Se_{0.06}$, emphasising the spectral range below 12000 cm^{-1}. With respect to Fig. 3, $\sigma_1(\omega)$ for both axes is shown here on an extended energy interval, in order to account for its substantial temperature dependence observed up to about 10^4 cm^{-1}. Insets: $\sigma_1(\omega)$ at 10 and 300 K with logarithmic energy scale showing the broad metallic (Drude) component (see text). Thick dashed lines are the total fit after the phenomenological Lorentz-Drude approach[18], while the thin lines display the single fit components at low frequencies (orange: Drude; green and brown: harmonic oscillator). The T-color code is identical in both panels and insets.

evolution, which is of interest here. We first introduce the quantity of the integrated spectral weight, defined as $SW(\omega) = \int_0^{\omega} \sigma_1(\omega')d\omega'$, where the cut-off frequency ω varies throughout the entire measured frequency range[18]. The insets of Fig. 5 and 6 show this quantity at 10 and 300 K below 10^4 and 1.5x10^4 cm^{-1} for $x = 0.01$ and 0.06, respectively, when ω continuously increases from zero up to the upper limit of our measurement. The SW reshuffling extends up to energy scales of the order of 1 to 2 eV, where its full recovery is achieved.

We are particularly interested to the SW distribution as a function of temperature. The first finding is that SW for both investigated compounds, along both axes tends to accumulate into the MIR-FIR spectral range upon lowering the temperature from 300 to 150 K. Below 150 K, the presence of CDW fluctuations and the proxim-

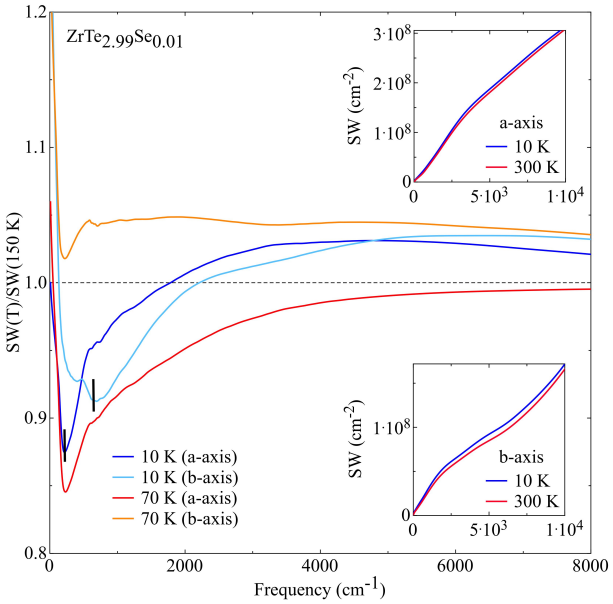

FIG. 5: (color online) Ratio of the integrated spectral weight $SW(T)/SW(150K)$ (see text) at selected temperatures along the a- and b-axis of $ZrTe_{2.99}Se_{0.01}$, emphasising the spectral range below 8000 cm^{-1}. Vertical bars identify the low temperature CDW (partial) gap. Insets: SW at 10 and 300 K below 10^4 cm^{-1} along the a- and b-axis, respectively.

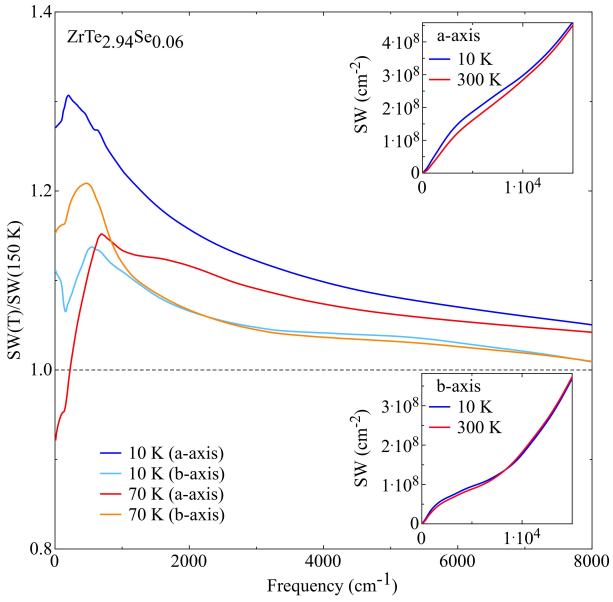

FIG. 6: (color online) Ratio of the integrated spectral weight $SW(T)/SW(150K)$ (see text) at selected temperatures along the a- and b-axis of $ZrTe_{2.94}Se_{0.06}$, emphasising the spectral range below 8000 cm^{-1}. Insets: SW at 10 and 300 K below 1.5x10^4 cm^{-1} along the a- and b-axis, respectively.

ity to the phase transition lead to a further redistribution of SW, which we now want to scrutinise. Towards this goal, we consider the ratio of $SW(T)$ at selected temperatures with respect to $SW(150K)$, as shown for both compounds in the main panel of Fig. 5 and 6 in the spectral range below 8000 cm^{-1}. The choice of 150 K as reference temperature is particularly ideal since it is yet representative for the normal state in both materials as well as not so far away from the CDW critical temperature, at least for the $x = 0.01$ compound.

Before going any further, it is worth pointing out a few general notions, as far as the expectations from the analysis of $SW(T)/SW(150K)$ are concerned. This ratio emphasises the relevant energy scale of SW transfer. If there is a transfer of SW from high to low energy, the SW ratio will exceed 1 at low energies and then smoothly approach 1 upon increasing ω until the full energy scale of the low-energy resonance is reached. For instance, SW may move into the low energy metallic (Drude) mode. If there is a transfer of SW from low to high energies (as it would occur by the opening of a CDW (partial) gap), the SW ratio will fall below 1 until the total energy scale of SW transfer is reached. The SW ratio will then display a depletion and its minimum defines the energy scale of the (CDW) single-particle (partial) gap excitation[18]. The SW redistribution is thus a powerful instrument in order to identify the relevant energy scales, anticipating or signalling the emergence of the CDW precursor effects or collective state. Indeed, a multi-component fit within the Lorentz-Drude phenomenological approach could lead to the association of intrinsic energy scales (like the CDW (partial) gap) with the model dependent resonance frequency of the Lorentz harmonic oscillators, which is manifestly less reliable.

For $ZrTe_{2.99}Se_{0.01}$ (Fig. 5), SW along the b-axis gathers between 150 and 70 K into a narrow range below 200 cm^{-1}, denoting the effective metallic contribution to $\sigma_1(\omega)$, and also accumulates in the mid- and near-infrared range (i.e., between 1000 and 10^4 cm^{-1}). By further lowering the temperature below T_{CDW}, SW is removed from the metallic (Drude) term, which narrows further. Between 100 and 2000 cm^{-1} the SW ratio drops and goes well below one, which indicates the opening of a partial gap. The minimum in the SW ratio at 700-800 cm^{-1} signals the turning point in SW transfer, so that above this frequency SW accumulates when entering the MIR range. Along the a-axis, we observe an even more dramatic SW redistribution. In fact already between 150 and 70 K, the SW ratio emphasises the pseudogap opening. At 70 K the metallic (Drude) contribution has narrowed considerably below 100 cm^{-1} and simultaneously there is a clear depletion in SW, reaching a maximal suppression around 200-300 cm^{-1}. This is followed by SW transfer to high frequencies. This trend further persists below 70 K upon entering the CDW phase. Down to 10 K, the SW of the metallic contribution to $\sigma_1(\omega)$ accumulates in a narrow frequency range. Again, a partial gap feature is clearly seen and additional SW from high energy scales even piles up into the MIR

range. The temperature dependence of SW, unfolded here, indicates the pseudogap formation at FS along the a-axis already above T_{CDW}. Such a pseudogap seems to merge into a CDW single particle (partial) gap below T_{CDW}, now for both axes. Taking the minimum in $SW(10K)/SW(150K)$ as an indicative estimation of the CDW (partial) gap (vertical bars in Fig. 5), we find a broad agreement with its magnitude in $ZrTe_3$[10,16]. The ratio $2\Delta_{CDW}/k_BT_{CDW} \sim 10$ and 20 at 10 K along the a- and b-axis, respectively, is substantially larger than 3.52 in the weak-coupling limit. This signals a break-down of the simple mean-field scenario and the presence of important fluctuation effects. Large gaps would indeed imply a mean-field transition temperature $T^{MF}_{CDW} > T_{CDW}$, besides strong electron-phonon coupling. This is similar to our findings in Ni- and Cu-intercalated $ZrTe_3$[16]. It is worth mentioning that detailed ARPES studies[20] as well as our early optical investigation[10] on $ZrTe_3$ equally show the formation of a pseudogap already at temperatures above T_{CDW} and demonstrate the relevant role of CDW fluctuation in a metallic CDW system.

For $ZrTe_{2.94}Se_{0.06}$ (Fig. 6), upon lowering the temperature, we observe an important reshuffling of SW from high frequencies (i.e., $5000 < \omega < 1.2\text{x}10^4$ cm^{-1}) into the strong absorptions between 600 and 2000 cm^{-1} along the a-axis and at 600 cm^{-1} along the b-axis. Along the a-axis there is even an incipient pseudogap formation with a tiny removal of SW below 200 cm^{-1} between 150 and 70 K (i.e., $SW(70\text{ K})/SW(150\text{ K}) < 1$). Upon further lowering the temperature to 10 K the metallic nature gets stronger and the overall Drude resonance dominates the spectrum. Along the b-axis, the metallic (Drude) resonance essentially narrows and its SW gets redistributed around 600 cm^{-1} from 70 to 10 K, yet in a too weak fashion to allow a true gapping of FS (i.e., $SW(10\text{ K})/SW(150\text{ K})$ does not go below 1).

V. CONCLUSION

The low-energy spectrum of the Se-doped $ZrTe_3$ is shaped by rather strong electronic absorptions at infrared energy scales. The integrated spectral weight, extracted from $\sigma_1(\omega)$, provides evidence for the formation of a pseudogap at the same energy scales at high temperatures along the a-axis for both investigated materials. The picture emerging from these investigations is not surprising and may be considered as a rather generic behavior of genuine CDW materials. Conversely, the novel aspect resides in the persistence of CDW features across the whole phase diagram, even for doping without a nominal CDW transition; an aspect, which was not possible to address and to appreciate in our previous works[10,16]. Such a pseudogap evolves into a (partial) CDW gap for $ZrTe_{2.99}Se_{0.01}$, affecting both crystallographic axes at $T < T_{CDW}$. Below 70 K, the gap feature is yet anisotropic but temperature independent. In $ZrTe_{2.94}Se_{0.06}$, the pseudogap substantially weakens or totally disappears upon lowering the temperature. This may be consistent with the tendency in these materials to form short range order, uncorrelated CDW segments at higher doping which then crossovers into a coherent CDW state at low doping. Our findings are in broad agreement with conjectures that doping perturbs the long-range phase coherence and induces patches of the CDW condensate[17]. Consequently, the electron scattering mechanism is dominated by local CDW fluctuations also existing outside the phase boundary of the CDW order. This leads to a substantial broadening of the Drude resonance as observed in $ZrTe_{2.94}Se_{0.06}$ (insets in Fig. 4), indicating an enhancement of the scattering rate of the itinerant charge carriers at large Se-doping content. We therefore confirm that effects due to the proximity of the CDW broken-symmetry state extend across a great portion of the phase diagram ($0 \leq x \leq 0.06$)[17] and we establish their impact up to temperatures of the order of 100 K. It remains to be seen whether CDW fluctuations could be invoked in the pairing mechanism and thus mediate the onset of superconductivity. Independently from this latter issue, our optical results do bear clear testimony for a pseudogap phase, preceding the onset of superconductivity. Therefore, our conclusions on model materials like the title compounds reinforce the notion that the pseudogap phase is far more generic to phase diagrams with competing broken-symmetry states and not an exclusive feature of cuprates.

Acknowledgments

This work has been supported by the Swiss National Foundation for the Scientific Research. Work at Brookhaven is supported by the U.S. DOE under Contract No. DESC00112704. Work at Institute of Solid State Physics of CAS is supported by the National Natural Science Foundation of China, Grant No. 11404342. Work at High magnetic field lab (Hefei) was supported by the National Key Research and Development Program of China (Grant No. 2017YFA0403502), and Youth Innovation Promotion Association of CAS(2017483). L.D. acknowledges the hospitality at KITP (University of California at Santa Barbara) within the Intertwined 2017 Programme, where part of this paper was elaborated.

Present address:
$^+$National Center for Catalysis Research, Indian Institute of Technology-Madras, Chennai 600036, Tamilnadu, India

[1] R.E. Peierls, Quantum Theory of Solids, Clarendon Press, Oxford (1955).

[2] G. Grüner, Density Waves in Solids, Addison Wesley, Reading, MA (1994).

[3] R. Daou, J. Chang, D. LeBoeuf, O. Cyr-Choinière, F. Laliberté, N. Doiron-Leyraud, B.J. Ramshaw, Ruixing Liang, D.A. Bonn, W.N. Hardy, and L. Taillefer, Nature **463**, 519 (2010).

[4] G. Ghiringhelli, M. Le Tacon, M. Minola, S. Blanco-Canosa, C. Mazzoli, N.B. Brookes, G.M. De Luca, A. Frano, D.G. Hawthorn, F. He, T. Loew, M. Moretti Sala, D.C. Peets, M. Salluzzo, E. Schierle, R. Sutarto,G.A. Sawatzky, E. Weschke, B. Keimer, and L. Braicovich, Science **337**, 821 (2012).

[5] J. Chang, E. Blackburn, A.T. Holmes, N.B. Christensen, J. Larsen, J. Mesot, Ruixing Liang, D.A. Bonn, W.N. Hardy, A. Watenphul, M. v. Zimmermann, E.M. Forgan, and S.M. Hayden, Nature Phys. **8**, 871 (2012).

[6] E. Blackburn, J. Chang, M. Hücker, A.T. Holmes, N.B. Christensen, Ruixing Liang, D.A. Bonn, W.N. Hardy, U. Rütt, O. Gutowski, M. v. Zimmermann, E.M. Forgan, and S.M. Hayden, Phys. Rev. Lett. **110**, 137004 (2013).

[7] R. Comin, A. Frano, M.M. Yee, Y. Yoshida, H. Eisaki, E. Schierle, E. Weschke, R. Sutarto, F. He, A. Soumyanarayanan, Y. He, M. Le Tacon, I.S. Elfimov, J.E. Hoffman, G.A. Sawatzky, B. Keimer, and A. Damascelli, Science **343**, 390 (2014).

[8] S.V. Borisenko, A.A. Kordyuk, V.B. Zabolotnyy, D.S. Inosov, D. Evtushinsky, B. Büchner, A.N. Yaresko, A. Varykhalov, R. Follath, W. Eberhardt, L. Patthey, and H. Berger Phys. Rev. Lett. **102**, 166402 (2009).

[9] S. Takahashi, T. Sambongi, J.W. Brill, and W. Roark, Solid State Commun. **49**, 1031 (1984).

[10] A. Perucchi, L. Degiorgi, and H. Berger, Eur. Phys. J. B **48**, 489 (2005).

[11] H. Nakajima, K. Nomura, and T. Sambongi, Physica B+C **143**, 240 (1986).

[12] R. Yomo, K. Yamaya, M. Abliz, M. Hedo, and Y. Uwatoko, Phys. Rev. B **71**, 132508 (2005).

[13] X. Zhu, H. Lei, and C. Petrovic, Phys. Rev. Lett. **106**, 246404 (2011).

[14] H. Lei, X. Zhu, and C. Petrovic, Europhys. Lett. **95**, 17011 (2011).

[15] C.S. Yadav and P.L. Paulose, J. Phys.: Condens. Matter **24**, 235702 (2012).

[16] C. Mirri, A. Dusza, X. Zhu, H. Lei, H. Ryu, L. Degiorgi, and C. Petrovic, Phys. Rev. B **89**, 035144 (2014).

[17] X. Zhu, W. Ning, L. Li, L. Ling, R. Zhang, J. Zhang, K. Wang, Y. Liu, L. Pi, Y. Ma, H. Du, M. Tian, Y. Sun, C. Petrovic, and Y. Zhang, Scientific repots **6**, doi:10.1038/srep26974 (2016).

[18] M. Dressel and G. Grüner, in *Electrodynamics of Solids*, Cambridge University Press (2002).

[19] The performed analysis (insets of Fig. 3 and 4) with a set of Drude-Lorentz components broadly agrees and supports the more general discussion and conclusions on the *SW* (re)-distribution.

[20] T. Yokoya, T. Kiss, A. Chainani, S. Shin, and K. Yamaya, Phys. Rev. B **71**, 140504(R) (2005).